NANO LETTERS

Letter

pubs.acs.org/NanoLett

Large-Area Nanosphere Self-Assembly by a Micro-Propulsive Injection Method for High Throughput Periodic Surface Nanotexturing

Pingqi Gao,[†] Jian He,[†] Suqiong Zhou,[†] Xi Yang,[†] Sizhong Li,[†,‡] Jiang Sheng,[†] Dan Wang,[†] Tianbao Yu,[‡] Jichun Ye,*[,†] and Yi Cui*[,§]

[†]Ningbo Institute of Material Technology and Engineering, Chinese Academy of Sciences, Ningbo, 315201, People's Republic of China

[‡]Department of Physics, Nanchang University, Nanchang, 330047, People's Republic of China

[§]Department of Material Science and Engineering, Stanford University, Stanford, California 94305, United States

ABSTRACT: A high throughput surface texturing process for optical and optoelectric devices based on a large-area self-assembly of nanospheres via a low-cost micropropulsive injection (MPI) method is presented. The novel MPI process enables the formation of a well-organized monolayer of hexagonally arranged nanosphere arrays (NAs) with tunable periodicity directly on the water surface, which is then transferred onto the preset substrates. This process can readily reach a throughput of 3000 wafers/h, which is compatible with the high volume photovoltaic manufacturing, thereby presenting a highly versatile platform for the fabrication of periodic nanotexturing on device surfaces. Specifically, a double-sided grating texturing with top-sided nanopencils and bottom-sided inverted-nanopyramids is realized in a thin film of crystalline silicon (28 μm in thickness) using chemical etching on the mask of NAs to significantly enhance antireflection and light trapping, resulting in absorptions nearly approaching the Lambertian limit over a broad wavelength range of 375−1000 nm and even surpassing this limit beyond 1000 nm. In addition, it is demonstrated that the NAs can serve as templates for replicas of three-dimensional conformal amorphous silicon films with significantly enhanced light harvesting. The MPI induced self-assembly process may provide a universal and cost-effective solution for boosting light utilization, a problem of crucial importance for ultrathin solar cells.

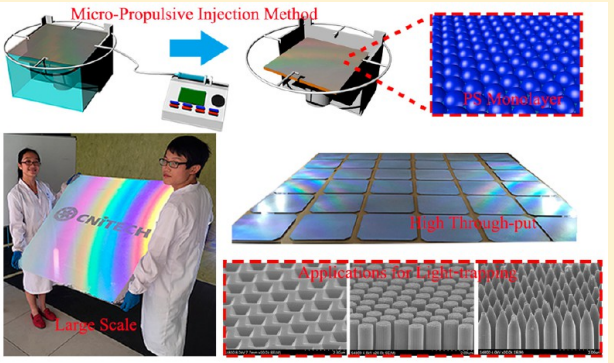

KEYWORDS: *Self-assembly, microsphere lithography, nanofabrication, light-trapping, photovoltaic*

Two-dimensional (2D) periodic nanostructure arrays have attracted intensive attention in the fields of photonics, electronics, biochemical sensing, and photovoltaics due to their excellent pattern-dependent properties.[1−6] For example, 2D periodic light-trapping nanostructures have been demonstrated to be effective to boost the light absorption of crystalline silicon (c-Si) thin-film solar cells, resulting in an energy conversion efficiency as high as its bulk counterpart with significantly reduced material and processing cost.[7−10] However, most of the patterning techniques for 2D periodic nanostructures, such as photolithography, electron beam lithography, X-ray lithography, soft lithography, and nanoimprinting,[11−14] do not have high throughput matching with the needs of high-volume manufacturing for the photovoltaic industry where a throughput of 2500−3000 wafers/h is typically needed and the cost control is very critical even down to a subpenny level.

Alternatively, the self-assembly approach that produces a monolayer of colloidal template has been verified to be an effective and versatile route toward functional 2D patterned nanostructures owing to its low cost, high reproducibility, and good controllability on the chemical composition and structural parameters.[15−19] A complete process to form a 2D template for conventional colloidal lithography (CL) should contain several steps in sequence: colloidal layer formation on a flat substrate by spin coating, layer transfer to a liquid surface, monolayer self-assembly at air/liquid interface, lift-up process, and monolayer formation on a target substrate. The quality of CL template is affected by every step, as well as by the hydrophilic/hydrophobic properties of the substrates, both of which confine its applications mainly in lab researches. By now, the successful demonstration of using CL template toward scalable patterning applications, especially for photovoltaics, is still missing.

In this Letter, we presented a new patterning technique that can produce large-area periodic nanostructure arrays with an ultrahigh throughput in cost-competitive ways. A micro-propulsive injection (MPI) process was developed to directly

Received: March 28, 2015
Revised: June 1, 2015

DOI: 10.1021/acs.nanolett.5b01202
Nano Lett. XXXX, XXX, XXX−XXX

spread out over the water surface the polystyrene (PS) nanosphere colloidal solution that finally evolved into a 2D hexagonally close-packed monolayer of PS nanospheres at the air/water interface. A large-area PS monolayer, even beyond the size of a few square meters, can be readily achieved, through a fine control of several key parameters, including contact states between the injectors and the water surface, injection speeds, injector numbers, PS nanosphere and dispersant concentrations, and so forth. Sequentially, the PS monolayer was transferred on preset substrates by slowly declining the water or raising the substrates. Served as an etching mask for the 2D PS arrays, photonic nanostructures, such as nanopillar (NP), nanopencil (NPC), and inverted-nanopyramid (INP), were successfully fabricated using suitable wet chemical etchings on 28 μm thick c-Si films in wafer scale and their light-trapping properties were thoroughly characterized. The double-sided nanotexturing configuration with NPC arrays on the top side and INP arrays on the bottom side has obtained light absorption very close to the Lambertian limit over a broad wavelength range of 375−1000 nm and even beyond this limit under the longer wavelength. Besides, the MPI induced large-area 2D PS monolayers were also used as facile texturing templates for other thin film absorbers by deposition process to boost the light harvesting.

The formation process of the PS monolayer of nanospheres is schematically shown in Figure 1, including the following series of steps: (1) presetting the substrates underneath the water and connecting the injectors with the MPI system (Figure 1a); (2) tuning the contact states between the injectors and the water surface and then initiating the MPI for the injection of PS colloids (Figure 1b); (3) turning off the MPI until a colorful interference pattern (an indicator of the formation of tightly self-assembled PS-monolayer) is formed on the entire water surface when illuminated by a white light source (Figure 1c); (4) slowly declining the water level or raising the substrate to transfer the PS monolayer onto the preset substrates (Figure 1d). Figure 1e shows a design concept of prototype MPI equipment with ultrahigh throughput for possible high-volume manufacturing application, which will be further discussed later.

The fabrication process outlined above will now be further described in more detail. First, ethanol, as a dispersant, is added to the water-based PS colloidal solution to lower the surface tension, which enables the more effective spreading of PS nanospheres on the water surface. The amount of ethanol additive is determined by the size and concentration of the nanospheres. This mixture is then sonicated for several minutes and continuously injected onto the water surface through the MPI system. The driving force for the spreading of PS nanospheres is associated with the Marangoni effect, a mass transfer along the interface between two fluids as a result of surface tension gradient.[20] In this case, as schematically shown in Figure 2a, when the injected ethanol-contained PS colloidal solution contacts the water surface the strong Marangoni forces are formed, pushing the colloidal particles to disperse outward rapidly from the regions with low surface tension, until they cover the whole surface of the water bath. Figure 2b shows a photograph of the real-time injection process in its initial stage (under white light illumination). The occurrence of colorful interference patterns around the needle tip shows that the monolayer formation begins as soon as the PS nanospheres are dropped onto the water surface and continues as they spread out over the water bath. It is worth noting that a meniscus

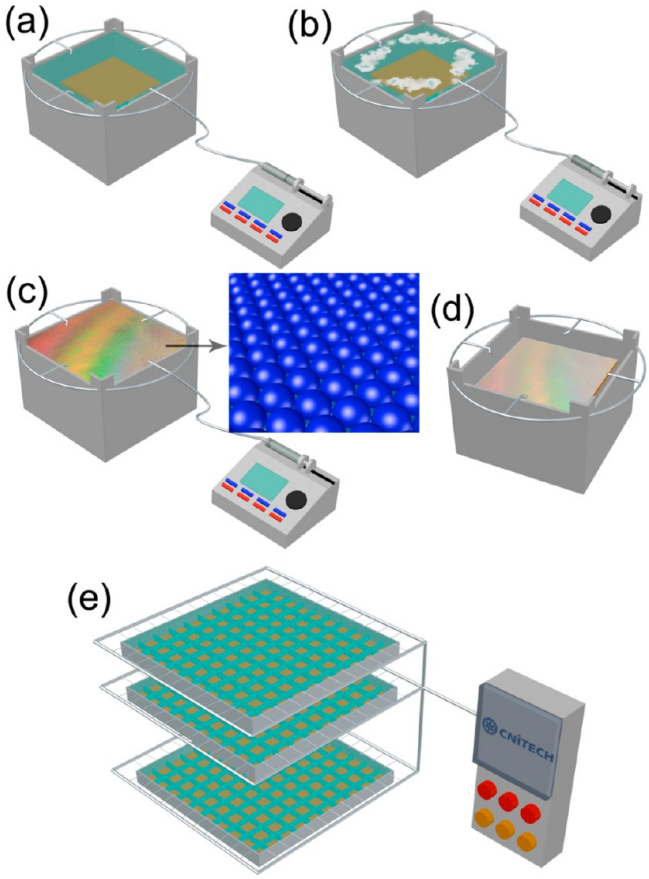

Figure 1. Schematics of the MPI systems and the formation processes for large-area PS nanosphere arrays in both of the lab scale (a−d) and manufacturing scale (e). (a) An MPI system with one injector and four nozzles. A substrate is preset underneath the water. (b) Initial stage for the injection of PS colloids over the water surface. (c) The formation of hexagonally arranged PS monolayer upon the water surface once a defectless and colorful interference pattern occurred under white light illumination. The inset image schematically shows the arranged PS monolayer. (d) Transfer of the PS-monolayer onto the preset substrates by slowly declining the water level or raising the substrate. (e) Design concept of a prototype MPI equipment in manufacturing scale. A few large-sized water baths are used with numerous injectors for each of the baths.

configuration along the needle tip is formed, as shown in Figure 2a,b, due to the surface tension of the water. This meniscus damps the vertical flow forces to prevent the break of the water surface, enabling the layering of the colloidal nanospheres on the water surface and immediately spreading out with the help of the dispersing agent of ethanol. The nozzle must be strictly positioned to be just in contact with the water surface. In addition, the dynamic and equilibrium conditions of the interface are also dependent on the injection speed, which must be carefully controlled below a certain value, in order to prevent sedimentation of the PS colloids caused by overmuch injection. Theoretically, the PS monolayer can be fabricated as large as possible by simply enlarging the surface areas of the deionized water, and as fast as possible by increasing the number of the injectors. For the MPI system with multiple injectors, the consistently clockwise (or anticlockwise) arrangement of all the injectors can accelerate the monolayer formation and avoid possible sedimentations caused by convective turbulences. Once the monolayer is formed, it is transferred

DOI: 10.1021/acs.nanolett.5b01202
Nano Lett. XXXX, XXX, XXX−XXX

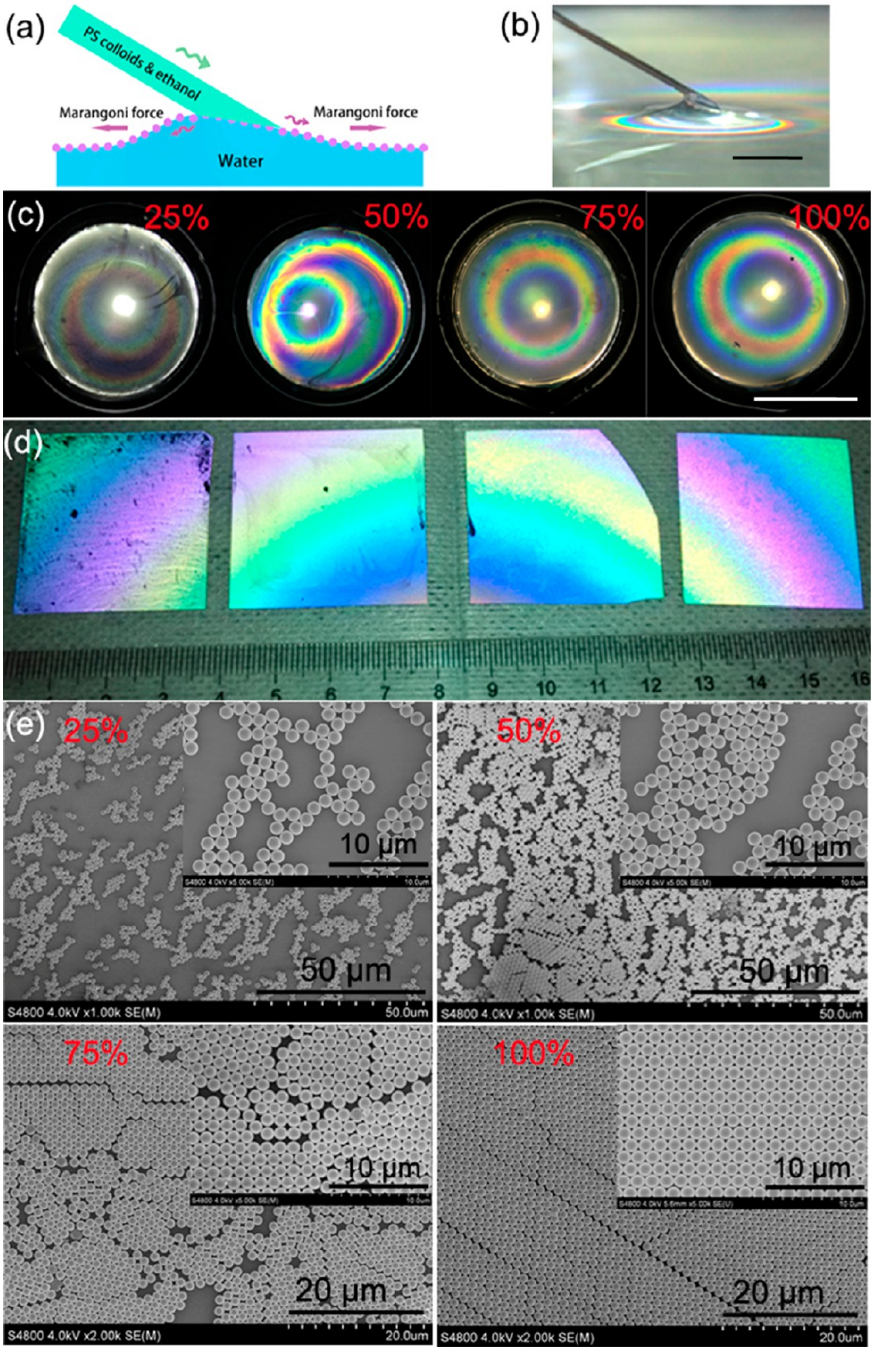

Figure 2. Procedure of preparation of close-packed PS monolayer on a substrate. (a) Schematics of the dynamic and equilibrium behaviors near the interface between the injector tip and the water surface. The colloidal solution together with ethanol are spread on the water surface through the nozzle, and then spread out under the driving of the Marangoni forces that are introduced by surface tension gradient. (b) A photograph of the real-time injection process in its initial stage. (c,d) The changes in iridescent images of PS nanospheres on water surfaces and Si substrates corresponding to different monolayer formation stages with PS area fraction of 25, 50, 75, and 100%, respectively. (e) SEM images corresponding to the four stages showed in (d). The scale bar in (b) is 0.5 cm and in (c) is 5 cm.

to submerged substrates by draining the water bath or raising the substrates slowly. As the solvent evaporates by self-evaporation or low-temperature baking (below 60 °C in our case), capillary forces draw the nanospheres together, and the nanospheres pack in a hexagonally close-packed pattern, tightly attaching on the substrates.

Macroscopically, the mechanism of forming PS monolayer on the water surface is based on the well-known Langmuir–Blodgett (LB) effect.[21−23] In this process, the PS nanospheres are continuously added by MPI until the area fraction of PS monolayer approaches 100%. The photographs of the water surfaces, the photographs of the silicon substrates, and the scanning electron microscopy (SEM) images of PS nanospheres on the silicon substrates are shown in Figure 2 panels c, d, and e, respectively, at various stages with the PS area fraction of 25, 50, 75, and 100%. As shown in Figure 2c, when the area fraction increases from 25 to 100%, the color fringes caused by diffraction from the PS arrays (upon white light illumination) become more distinct and more uniform with more area coverage of the wafer surface, indicating that the PS

DOI: 10.1021/acs.nanolett.5b01202
Nano Lett. XXXX, XXX, XXX−XXX

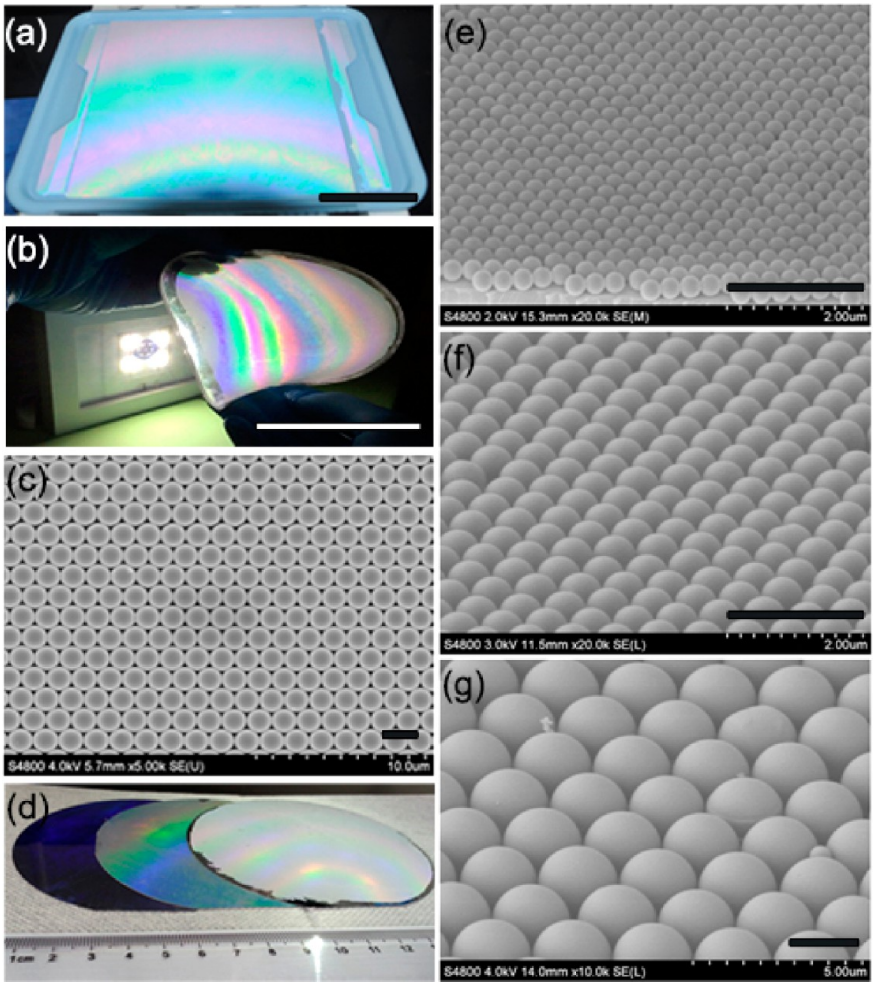

Figure 3. Demonstrations of the MPI-induced PS monolayers. (a) Photograph of as-deposited PS monolayers on glass (in middle part) and on uneven plastic substrate (at left and right edges) just after drained water. (b) Photographs of PS monolayers on PDMS substrates. (c) SEM image of the well-arranged PSs from the glass substrate in (b); the diameter of this PS is 1400 nm. (d–g) Photograph and SEM images collected from other three types of PS monolayers with diameters of 300, 700, and 2000 nm. The scale bar in (a,b) is 10 cm and in (c,e–g) is 2 μm.

nanospheres evolve from a randomly discrete arrangement to a regularly packed array pattern. This trend can also be confirmed by the optical images (Figure 2d) and the SEM images (Figure 2e) of the silicon substrates with the transferred PS nanospheres from the various stages. The SEM image for the monolayer assembly of the PS nanospheres with 100% area fraction shows nearly defect-free arrays, except for a few vacancies and slip dislocations, as in all crystal materials.

It is worth noting that this process has a high tolerance to large surface roughness. Figure 3a shows the image of a flat glass (30 × 30 cm in square) and an underneath plastic holder (30 × 40 cm in area). The whole area of the flat glass and the unshielded part of the plastic holder are fully covered by the PS nanospheres, exhibiting uniform colorful diffraction fringes. Although the integrity is interrupted by the step height between the glass surface and plastic surface, the monolayer of PS nanopheres can still be well formed on each part of surfaces without any disturbance of the internal hexagonally ordered arrays. Moreover, this self-assembled monolayer of PS nanospheres can be transferred to various substrates, regardless of their hydrophilic/hydrophobic natures of the surface. For example, the PS arrays of nanospheres can be readily transferred to the Si wafer (Figure 2d) and the flexible polydimethylsiloxane (PDMS) film (Figure 3b). Once the solvent is evaporated, the PS nanospheres adhere to the substrate surface tightly and even the bending of the flexible PDMS (Figure 3b) will not damage the well packed monolayer. Furthermore, this process is capable to assemble nanospheres with tunable diameters, broadening the applications as a physical mask in the colloidal lithography process. In addition to the above-mentioned 1400 nm PS nanospheres (Figure 3a–c), the Si substrates covered with PS monolayer of nanospheres in the diameters of 300, 700, and 2000 nm are also shown in Figure 3d, where these samples show different colors upon white light illumination with the PS nanospheres of 300 nm showing the dark blue color due to the diffraction of the short wavelength. The SEM images in Figure 3e–g for these three types of PS nanospheres further make sure that our MPI method is powerful for a larger span on the PS nanospheres.

As illustrated in Figure 1e, this simple assembly technique induced by MPI process can readily reach a high throughput via a streamlined batch process, where large-sized water baths are used with numerous injectors for each of the bath. From this design configuration, a throughput of 3000 wafers/h (156 × 156 mm for each wafer) can be readily achieved if 30 water baths (2.5 m^2 for each bath) are used vertically with a streamlined automation to save the footprint of the tool. Figure 4 demonstrates our capability in fabricating PS monolayer over

DOI: 10.1021/acs.nanolett.5b01202
Nano Lett. XXXX, XXX, XXX–XXX

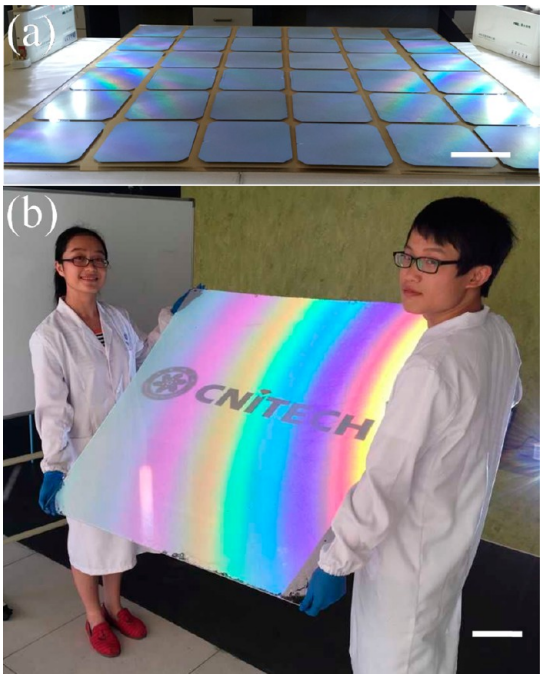

Figure 4. Photographs of as-deposited PS monolayer on (a) 36 wafers and (b) 1 m^2 glass substrate. The water bath used here is 1.3 × 1.3 cm^2. The scale bar in (a,b) is 10 cm.

large area (1 × 1 m^2 on glass) and in high throughput (6 × 6 wafers), respectively. The parameters of MPI processes in this lab scale, respectively. The parameters of MPI processes in this lab scale and a hypothetical manufacturing scale are summarized in Table 1, if the same PS colloidal solution (for the 1400 nm-PS case, 2.5 wt % colloidal solutions were used with 1:1 ethanol to solution in volume) and same injection rate (0.5 mL/h) are assumed. In the lab scale process, it took 4 h to form a PS monolayer over the 130 × 130 cm area (1.7 m^2) with 25 nozzles. As a comparison, for the manufacturing scale process, 4400 nozzles are needed to realize the throughput of 3000 wafers/h, making it a viable process for the advanced surface texturization for the photovoltaic industry. Note that the number of required water baths can be further reduced, for example, to 15 if 8800 nozzles are used. In the next a few paragraphs, two cases are adopted to demonstrate the practical use of the MPI process to fabricate the periodic patterns of surface texturing to greatly enhance light trapping for the solar cell applications.

To use thin c-Si films as active materials is a potential approach to significantly lower the cost of c-Si solar cells, and equivalent efficiencies to their bulk counterpart have been theoretically and experimentally demonstrated on c-Si films with the thickness ranging from 20 to 40 μm.[24,25] The use of thin c-Si films allows lower quality Si with shorter carrier diffusion lengths to be adopted to maintain the high performance. The thin c-Si films can also minimize Auger recombination, leading to larger open circuit voltages and fill-factors.[25] Furthermore, lightweight and flexibility of the thin c-Si solar cells expand the applications to the military, aerospace, and other special circumstances. Unfortunately, with the reduction in thickness thin c-Si films suffer from a significantly reduced optical absorption, especially in the red and near-infrared regions of the solar spectrum. The traditionally used light-trapping scheme in conventional standard wafer-based c-Si solar cells (typically 160−200 μm) usually exploit random pyramid texturing combined with an antireflection coating (ARC) layer on the front side and a metallic back reflector on the back side to supply an overall reflectance of approximately 5−6% in wavelengths range of 300−1200 nm. However, this light-trapping scheme might not be suited for the thin cells particularly when the cell thickness is comparable to the dimensions of pyramidal textures (3 to 10 μm). As an effective alternative, the artificial 2D photonic crystals with nanoscale modulations of the refractive index, including nanopyramid (or inverted nanopyramid),[8] nanohoneycomb,[26] nanocone,[9,27] nanowire/nanohole,[28,29] have been successfully demonstrated to significantly improve the light absorption by reducing reflection and increasing optical path.

When combined with other fabrication methods, such as wet etching (acid or alkaline), reactive ion etching (RIE, for spatial opening between the PS nanospheres), metal-assisted chemical etching (MaCE), and so forth, the MPI-induced periodic PS monolayers can be readily used as CL masks to produce various nanophotonic texturing on c-Si thin films. Here, several light-trapping schemes of single-sided texturing with arrays of nanopillars (NPs), nanopencils (NPCs), and inverted-nanopyramids (INPs) and a double-sided texturing with top-sided NPCs and bottom-sided INPs are demonstrated experimentally on thin c-Si films with the thickness of 28 μm. The fabrication details are described in the part of Methods. Figure 5a−c shows the SEM images of hexagonal arrays of INPs, NPs, and NPCs, respectively. The periodicity, diameter, and height of the NP array are about 900, 800, and 2000 nm, respectively, and they are separately controlled by the diameter of PS nanospheres, RIE-etching and wet-etching time, respectively. The NPCs are evolved from the NPs via a reconstruction process by MaCE, so that they have similar periodicity (900 nm), bottom diameter (800 nm), and depth (2000 nm) to the NPs. The INP array has a periodicity of 1400 nm and a height of about 600 nm with the target for light trapping roughly in the 800−1100 nm wavelength range. A fill factor for the open areas of the INPs over the entire surface is estimated to be 0.7 for the sample showed in Figure 5a.

The light-trapping properties are studied through reflection spectra measurement on the c-Si films (28 μm) with various surface texturing, bottom-sided INPs patterning (in green), top-sided NPs patterning (in blue), top-sided NPCs patterning (in red), and flat thin film as a reference (in black), as shown in Figure 5d. Compared to the flat film, a noticeable reflection reduction is observed in the bottom-sided INPs sample for the wavelengths beyond 800 nm. In this long wavelength range, the light absorption in Si is typically insufficient due to the low

Table 1. Summarization of the Parameters for the Deposition of 1400 nm PS Monolayers Using the MPI Processes in Both of the Lab Scale and Manufacturing Scale

	deposition area (m^2)	PS solution consumption (mL)	injector numbers	injection rate (mL/h)	duration time (h)
lab scale	1.7	50	25	0.5	4
manufacturing scale	75 (3000 wafers)	2200	4400	0.5	1

DOI: 10.1021/acs.nanolett.5b01202
Nano Lett. XXXX, XXX, XXX−XXX

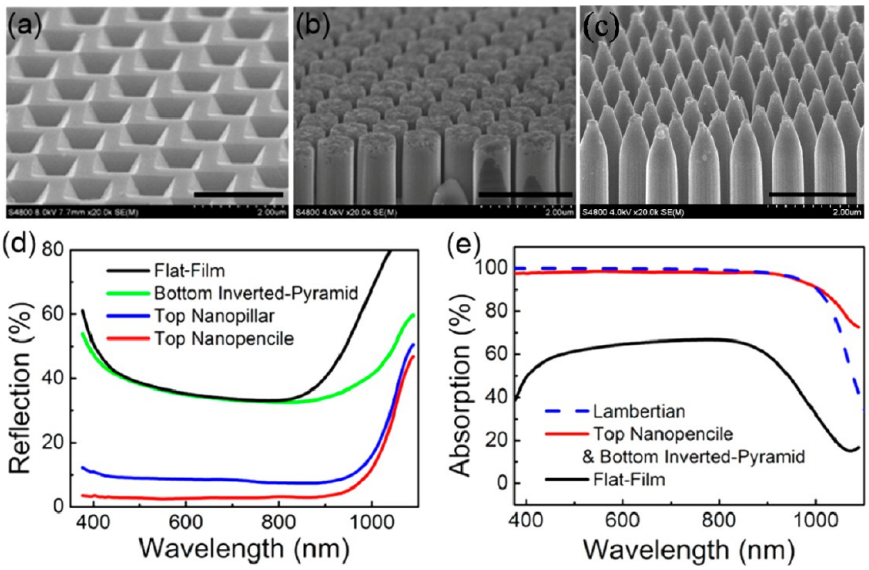

Figure 5. Several periodic surface texturing structures that are fabricated by using the PS monolayers as templates and their light trapping properties on c-Si thin film. (a–c) SEM images of an inverted-nanopyramid (INP) array, a nanopillar (NP) array, and a nanopencil (NPC) array. (d) The reflection spectrum of a flat 28 μm thick c-Si thin film without any surface textures (black) with bottom-INPs patterning (in green), with top-NPs patterning (in blue), and with top-NPCs patterning (in red), respectively. (e) The absorption spectrum of a 28 μm thick c-Si thin film with double-sided grating texturing (top-NPC array and bottom-INP array). The INP arrays have a periodicity of 1400 nm, and the NP and NPC arrays have the same periodicity of 900 nm. The scale bar in (a–c) is 2 μm.

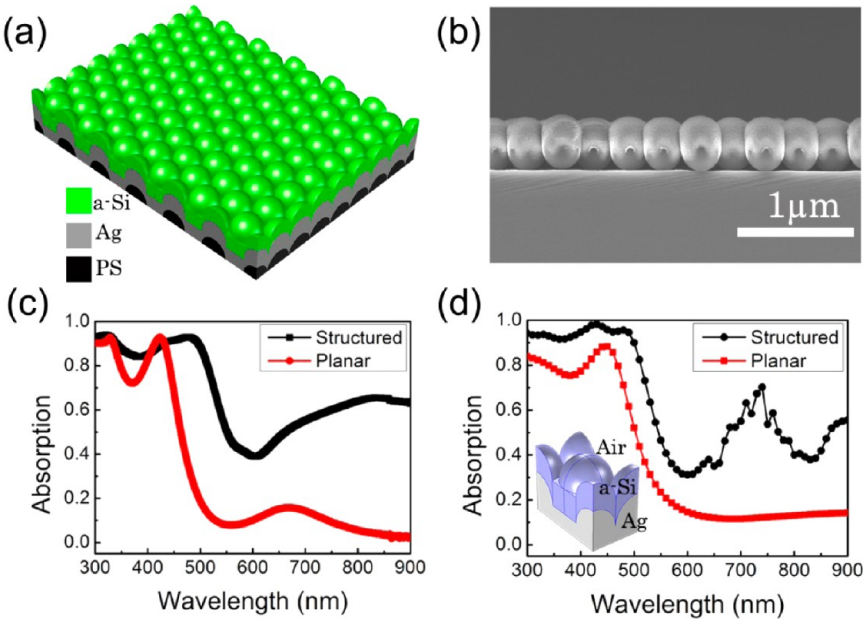

Figure 6. Light absorption characterizations of thin a-Si films on PS monolayers. (a) Schematic of the 3D layered structure. (b) Cross-sectional SEM image for the same structure in (a). (c,d) Absorption spectra of a structured and a flat a-Si film with the same thickness of 160 nm; measurements in (c) and simulations in (d). Inset in (d) shows the unit cell configuration that is used for simulation. The diameter of the PS nanospheres is 300 nm.

absorption coefficients and thus the unabsorbed lights can easily reach the rear surface and interact with the INPs with an optically matched feature size, resulting in a significant diffraction which reduces the chance for the light to escape from the front surface to air due to the increased light path inside the c-Si and the higher probability of internal reflection at top Si/air surface. As reported, the light with the wavelength below 800 nm can be completely absorbed by a ~28 μm thick Si film, and thus there is no enhancement in light absorption confirming that the texturing on the rear surface does not directly contribute to antireflection.[30] For the texturing schemes on the top surface, both the NPs and NPCs, substantial reflection reductions are observed over the entire usable solar spectrum. The average reflection among the range 375–900 nm dramatically decreases from 38% for flat film to 8.8% for the sample with NP texturing, and then further drops to 2.9% for the sample with NPC texturing. The periodicity of the NP and NPC arrays is in the subwavelength regime, which making an effective averaged index for the incoming light and help to achieve effective antireflection. The minimum reflection for the sample with NPs occurs exactly at the wavelength of 900 nm, which is equal to the periodicity of the arrays, indicating an

DOI: 10.1021/acs.nanolett.5b01202
Nano Lett. XXXX, XXX, XXX–XXX

enhanced light scattering occurs over there. Furthermore, the sample with NPCs shows a greatly enhanced antireflection when compared to the one with NCs. This is attributed to its gradual structural change on the top part of NPs, which provides a smooth index transition from air to silicon, that is, an excellent impedance match.[31]

In order to boost the light absorption over the entire solar spectrum, a double-sided grating texturing with NPCs on the top side and INPs on the rear side is used to fully explore light trapping effect. The absorption spectrum of this new structure was measured, as shown in Figure 5e. The double-sided patterned sample shows an absorption (red curve) of above 97% at almost all the wavelengths in the range of 375−900 nm, nearly approaching the Lambertian limit (blue dashed curve). More interestingly, the absorption beyond 900 nm is found even to exceed the limit, demonstrating an outstanding light trapping performance for this double-sided texturing design. The absorption properties may be further improved by optimizing on the structural characters of the 2D gratings, including the periodicity, feature size, depth, and so forth. Because the NPC and the INP structures have relatively low aspect ratio and the less damaging wet etching process is used, the issues of surface recombination losses and degradation of electronic properties would be less severe than those with high aspect ratio nanoscale structures.

In addition to being used as masks for top-down etching on c-Si, the MPI induced monolayer of PS nanospheres can also be used as templates to conformally deposit thin films with a periodic array configuration in a bottom-up manner.[32] With this method, periodic amorphous silicon (a-Si) thin films are deposited on PS nanosphere arrays, and the light-trapping properties are investigated experimentally and theoretically. The schematic drawing and the cross-sectional SEM image of the structures are shown in Figure 6a,b. For high antireflection purpose, the PS monolayer with a periodicity of 300 nm is selected as the periodic substrates, the silver (Ag) layer and a-Si film with thickness of 200 and 160 nm, respectively, are successively deposited by sputtering. As shown in Figure 6c, the measured absorption spectrum of the a-Si film with a periodic configuration exhibited significantly enhanced absorption over the entire spectrum compared to the planar one, more specifically, an 71.6% enhancement in the overall absorptions (from 45.1 to 77.4%). The effective antireflection from the top surface, the reflection from bottom Ag reflector, and surface plasmon polaritons (SPPs) related effect from back-sided Ag-grating, jointly contribute to the absorption improvement. Figure 6d shows the simulated absorption spectra and they are well in accordance with the experimental results (Figure 6c). The absorption is primarily enhanced by a graded-refractive index profile of the top periodic surface that results in a broadband antireflection effect. For the wavelength beyond 500 nm, the a-Si layer is less absorptive and most of the incident light could not be efficiently absorbed in a single path. Thus, the back-reflection plays a more important role. While at the wavelength between 670 and 790 nm, the absorption peaks are directly ascribed to SPPs related scattering enhancement. This bottom-up periodically patterning scheme should be widely expanded to improve the optical performance of other thin film solar cells, such as cadmium telluride, copper−indium-gallium-selenide, perovskite, and so forth.

In summary, a high throughput process for assembling of large-area PS monolayers was presented based on a micro-propulsive injection method. The process and the resultant PS monolayers have four distinct characteristics: (1) large-area capability, (2) scalable throughput as high as 2500−3000 wafers/h, (3) tunable periodicity, and (4) compatibility to various types of substrates (from rigid to flexible, smooth to rough, hydrophilic to hydrophobic, and so forth). This low-cost and high-throughput process of PS monolayer assembling, delivering templates for advanced grating nanotexturing either on c-Si or a-Si films, provides an experimentally feasible strategy in efficiency improvement and cost reduction for thin solar cells.

Methods. *Thin Film c-Si Fabrication.* The ultrathin c-Si films were etched from one-side polished p-type (100) Si wafers (4 in. diameter, 200 μm in thickness, CZ), which were immersed in a KOH solution with a concentration of 50 wt % at 80 °C. The etching rate is about 80 μm/h. The final thickness of these thin films was judged by the transmittance color of the wafer upon the illumination of white light.

Bottom-Sided Inverted-nanopyramid Arrays Fabrication. Polystyrene (PS) nanospheres with the diameter of 1400 nm were used for the fabrication of back-side inverted-nanopyramid arrays. Detailed formation process of monolayers of nanospheres was shown in the main article. Subsequently, a reactive ion etching (RIE) system was used to reduce the diameter of PS nanospheres and thus a space between the spheres was created. Titanium (Ti) film with the thickness of ∼40 nm was then deposited by a magnetron sputtering system. The PS nanospheres were removed via sonication in methylbenzene and the remaining Ti is used as a hardmask for chemical etching toward the inverted-nanopyramids. After the immersion in the etchant solution (20 wt % NaOH and 20 wt % isopropanol in DI water) for 510 s, the inverted-nanopyramids were formed, and the samples were then thoroughly rinsed with DI water. Finally, the samples were immersed in 20 vol % HF to remove the residual Ti film.

Top-Sided Nanopillar Arrays Fabrication. The nanopillar structures were fabricated by an Au-assisted chemical etching process. The PS nanospheres with the diameter of 900 nm were used as etching mask as discussed in main article. After RIE process, the Si film covered with the monolayer of PS nanosphere was deposited with Ti/Au bilayer films (with the thickness of 1.5 and 20 nm, respectively) by electron beam evaporation system with the deposition rate of 0.1 and 1 Å/s, respectively. After the removal of the PS nanospheres via sonication in methylbenzene, the samples were immersed in etchant (HF (49%), H_2O_2 (31%), and H_2O at a volume ratio of 10:1:40) for 30 min at room temperature to form nanopillars with the assistance from the Au metal. The residual Au film was removed eventually in an etchant solution with 5% I_2, 10% KI, and 85% H_2O in room temperature.

Top-sided Nanopencil Arrays Fabrication. Nanopencil arrays were fabricated by an anisotropic etching of nanopillar arrays for multiple times using an Ag-assisted chemical etching process with the same etchant containing $AgNO_3$ (0.00017 M), HF (2 M), and HNO_3 (0.005 M).

Simulations of The Absorption Spectrum for Patterned a-Si. The unit cell of the structure is shown as inset in Figure 6d. The optical index of the a-Si is based on the ellipsometry measurement and the optical parameter of Ag is based on the Palik data.[33] The simulations are performed by finite element method within a unit configuration surrounded by the periodic boundaries along the lateral directions. The absorption at each wavelength is calculated with an interval of 10 nm.

DOI: 10.1021/acs.nanolett.5b01202
Nano Lett. XXXX, XXX, XXX−XXX

Optical Measurement. The optical characterization of the samples was carried out using spectrophotometer (Helios LAB-rc, with an integrating sphere) in the wavelength range of 375–1100 nm. For reflectance (R) measurement, a silver mirror covered with a 150 nm SiO_2 layer was placed underneath the c-Si thin films in order to avoid the parasitic absorption in the back-Ag reflector. Because the samples measured here have a Ag metal layer on the back to prevent light transmission, the absorptance (A) of the final structures can be simply calculated from the $A = 1 - R$, where R is the reflectance.

AUTHOR INFORMATION

Corresponding Authors

*E-mail: jichun.ye@nimte.ac.cn.
*E-mail: yicui@stanford.edu.

Notes

The authors declare no competing financial interest.

ACKNOWLEDGMENTS

We acknowledge financial support by Thousand Talent Program for Young Outstanding Scientists of People's Republic China, National Natural Science Foundation of China (Grant 61404144), Zhejiang Provincial Natural Science Foundation (Grant LY14F040005), Natural Science Foundation of Ningbo (Grant 2013A610030). Y.C. acknowledges the support from Bay Area Photovoltaic Consortium (BAPVC) funded by the U.S. Department of Energy Sunshot Innitiative.

REFERENCES

(1) Fan, Z.; Razavi, H.; Do, J.-w.; Moriwaki, A.; Ergen, O.; Chueh, Y.-L.; Leu, P. W.; Ho, J. C.; Takahashi, T.; Reichertz, L. A.; Neale, S.; Yu, K.; Wu, M.; Ager, J. W.; Javey, A. *Nat. Mater.* **2009**, *8*, 648–653.
(2) Kelzenberg, M. D.; Boettcher, S. W.; Petykiewicz, J. A.; Turner-Evans, D. B.; Putnam, M. C.; Warren, E. L.; Spurgeon, J. M.; Briggs, R. M.; Lewis, N. S.; Atwater, H. A. *Nat. Mater.* **2010**, *9*, 368–368.
(3) Henzie, J.; Barton, J. E.; Stender, C. L.; Odom, T. W. *Acc. Chem. Res.* **2006**, *39* (4), 249–257.
(4) Lei, Y.; Yang, S. K.; Wu, M. H.; Wilde, G. *Chem. Soc. Rev.* **2011**, *40* (3), 1247–1258.
(5) Ye, X. Z.; Qi, L. M. *Nano Today* **2011**, *6* (6), 608–631.
(6) Brongersma, M. L.; Cui, Y.; Fan, S. *Nat. Mater.* **2014**, *5* (13), 451–560.
(7) Cho, Y.; Gwon, M.; Park, H. H.; Kim, J.; Kim, D. W. *Nanoscale* **2014**, *6* (16), 9568–9573.
(8) Mavrokefalos, A.; Han, S. E.; Yerci, S.; Branham, M. S.; Chen, G. *Nano Lett.* **2012**, *12* (6), 2792–2796.
(9) Jeong, S.; McGehee, M. D.; Cui, Y. *Nat. Commun.* **2013**, *4*, 2950.
(10) Branham, M. S.; Hsu, W. C.; Yerci, S.; Loomis, J.; Boriskina, S. V.; Hoard, B. R.; Han, S. E.; Chen, G. *Adv. Mater.* **2015**, *13* (27), 2182.
(11) Gates, B. D.; Xu, Q. B.; Stewart, M.; Ryan, D.; Willson, C. G.; Whitesides, G. M. *Chem. Rev.* **2005**, *105* (4), 1171–1196.
(12) Geissler, M.; Xia, Y. N. *Adv. Mater.* **2004**, *16* (15), 1249–1269.
(13) Guo, L. J. *Adv. Mater.* **2007**, *19* (4), 495–513.
(14) Shir, D.; Yoon, J.; Chanda, D.; Ryu, J. H.; Rogers, J. A. *Nano Lett.* **2010**, *10* (8), 3041–3046.
(15) Trau, M.; Saville, D. A.; Aksay, I. A. *Science* **1996**, *272* (5262), 706–709.
(16) Lin, H.; Cheung, H. Y.; Xiu, F.; Wang, F. Y.; Yip, S. P.; Han, N.; Hung, T. F.; Zhou, J.; Ho, J. C.; Wong, C. Y. *J. Mater. Chem. A* **2013**, *1* (34), 9942–9946.
(17) Lin, H.; Xiu, F.; Fang, M.; Yip, S.; Cheung, H. Y.; Wang, F. Y.; Han, N.; Chan, K. S.; Wong, C. Y.; Ho, J. C. *ACS Nano* **2014**, *8* (4), 3752–3760.
(18) Yang, S. M.; Jang, S. G.; Choi, D. G.; Kim, S.; Yu, H. K. *Small* **2006**, *2* (4), 458–475.
(19) Hsu, C.; Connor, S. T.; Tang, M. X.; Cui, Y. *Appl. Phys. Lett.* **2008**, *93*, 133109 .
(20) Scriven, L. E.; Sternling, C. V. *Nature* **1960**, *187* (4733), 186–188.
(21) Kosiorek, A.; Kandulski, W.; Chudzinski, P.; Kempa, K.; Giersig, M. *Nano Lett.* **2004**, *4*, 1359–1363.
(22) Somobrata, A.; Jonathan, P. H.; Katsuhiko, A. *Adv. Mater.* **2009**, *21*, 2959–2981.
(23) Ho, C. C.; Chen, P. Y.; Lin, K. H.; Juan, W. T.; Lee, W. L. *ACS Appl. Mater. Interfaces* **2011**, *3*, 204–208.
(24) Green, M. A.; Emery, K.; Hishikawa, Y.; Warta, W.; Dunlop, E. D. *Prog. Photovoltaics* **2015**, *23*, 1–9.
(25) Bozzola, A.; Kowalczewski, P.; Andreani, L. C. *J. Appl. Phys.* **2014**, *115*, 094501.
(26) Gao, P.; Wang, H.; Sun, Z.; Han, W.; Li, J.; Ye, J. *Appl. Phys. Lett.* **2013**, *103*, 253105.
(27) Wang, K. X. Z.; Yu, Z. F.; Liu, V.; Cui, Y.; Fan, S. H. *Nano Lett.* **2012**, *12* (3), 1616–1619.
(28) Garnett, E.; Yang, P. *Nano Lett.* **2010**, *10*, 1082–1087.
(29) Trompoukis, C.; El Daif, O.; Depauw, V.; Gordon, I.; Poortmans, J. *Appl. Phys. Lett.* **2012**, *101*, 103901.
(30) Wang, S.; Weil, B. D.; Li, Y.; Wang, K. X.; Garnett, E.; Fan, S.; Cui, Y. *Nano Lett.* **2013**, *13* (9), 4393–4398.
(31) Herman, A.; Trompoukis, C.; Depauw, V.; El Daif, O.; Deparis, O. *J. Appl. Phys.* **2012**, *112*, 113107.
(32) Zhu, J.; Hsu, C. M.; Yu, Z. F.; Fan, S. H.; Cui, Y. *Nano Lett.* **2010**, *6* (10), 1979–1984.
(33) Palik, E. D. *Handbook of Optical Constants of Solids*; Academic Press: Orlando, 1998.

DOI: 10.1021/acs.nanolett.5b01202
Nano Lett. XXXX, XXX, XXX–XXX